Article

Influence of Metal Ions on the Structural Complexity of Mixed-Ligand Divalent Coordination Polymers

Fang-Ju Cheng , Kai-Min Wang , Chia-Yi Lee , Song-Wei Wang , Kedar Bahadur Thapa * , Manivannan Govindaraj * , Jhy-Der Chen *

Posted Date: 27 August 2024

doi: 10.20944/preprints202408.1890.v1

Keywords: coordination polymers; crystal structure; entanglement; dicarboxylic acid; bis-pyridyl-bis-amide

 doi:10.20944/preprints202408.1890.v1

Article

Influence of Metal Ions on the Structural Complexity of Mixed-Ligand Divalent Coordination Polymers

Fang-Ju Cheng [1], Kai-Min Wang [1], Chia-Yi Lee [1], Song-Wei Wang [1], Kedar Bahadur Thapa [2]*, Manivannan Govindaraj [3]* and Jhy-Der Chen [1]*

[1] Department of Chemistry, Chung-Yuan Christian University, Chung-Li 320, Taiwan; anncheng0327@gmail.com (F.-J.C.); g10663604@cycu.edu.tw (K.-M.W.); miss10031031@gmail.com (C.-Y.L.); bvbv20520@gmail.com (S.-W.W.)

[2] Makawanpur Multiple Campus, affiliated to Tribhuvan University, Municipality Rd, Hetauda, Nepal

[3] Department of Chemistry, Periyar Maniammai Institute of Science & Technology (Deemed to be University), Vallam, Thanjavur, 613 403, Tamil Nadu, India

* Correspondence: kedar.bthapa1977@gmail.com (K.B.T.); manivannang@pmu.edu (M.G.); jdchen@cycu.edu.tw (J.-D.C.); Tel.: +886-3-265-3351 (J.-D.C.)

Abstract: The reactions of the angular ligand 4,4′-oxybis(*N*-(pyridin-3-yl)benzamide (**L**^{1}) and 1,4-naphthalenedicarboxylic acid (1,4-H_2NDC) with divalent metal salts yielded three distinct coordination polymers (CPs): $\{[Zn_2(\mathbf{L}^1)(1,4\text{-NDC})_2]\cdot MeOH\}_n$, **1**, $\{[Cu(\mathbf{L}^1)(1,4\text{-NDC})(H_2O)]\cdot 3H_2O\}_n$, **2**, and $\{[Cd(\mathbf{L}^1)(1,4\text{-NDC})]\cdot 2H_2O\}_n$, **3**. Complex **1** features a 2-fold interpenetrated 3D framework with the $(4^{12}.6^3)$-**pcu** topology, while complex **2** reveals a 1D triple-strained helical chain, and complex **3** displays a 3-fold interpenetrated 3D framework with (6^6)-**dia** topology. Additionally, the reactions of the flexible ligand *N*,*N*′-bis(3-methylpyridyl)adipoamide (**L**^{2}) afforded $\{[Co_4(\mathbf{L}^2)_{0.5}(1,4\text{-NDC})_3(H_2O)_3(\mu_3\text{-OH})_2]\cdot EtOH\cdot 2H_2O\}_n$, **4**, $\{[Zn_2(\mathbf{L}^2)(1,4\text{-NDC})_2]\cdot 2CH_3OH\}_n$, **5**, and $[Cd(\mathbf{L}^2)(adipic)(H_2O)]_n$ (H_2adipic = adipic acid), **6**, exhibiting a self-catenated 3D framework with the $(4^{20}.6^8)$-8T32 topology, a 2D layer with the $(4^{13}\cdot 6^2)$-(4,4)IIb topology, and a 2D layer with the $(4^4\cdot 6^2)$-**sql** topology, respectively. The structural diversity observed in complexes **1** - **6** highlights the pivotal influence of the metal center on the degree of entanglement in CPs within mixed-ligand systems. The thermal stability and luminescent properties of complexes **1** - **3**, **4**, and **6** are also discussed.

Keywords: coordination polymers; crystal structure; entanglement; dicarboxylic acid; bis-pyridyl-bis-amide

1. Introduction

The synthesis of coordination polymers (CPs) has attracted significant attention within the research community, not only due to their potential as novel zeolite-like materials for applications such as separation, ion exchange, and catalysis, but also because of their diverse structural topologies [1,2]. The construction of CPs relies on suitable metal-ligand interactions and supramolecular forces [3], which are influenced by various reaction conditions, including metal-to-ligand ratios, solvent systems, and temperature [4–6]. Additionally, the intriguing entanglements observed in CPs, such as interpenetration, polycatenation, and self-catenation, arise from the interweaving of independent motifs in various configurations [7,8]. Despite numerous reports on entangled CPs, controlling structural dimensionality remains a key objective, and understanding the factors that govern this control continues to pose a significant challenge in the field of crystal engineering.

The flexible bis-pyridyl-bis-amide (bpba) ligands, known for their ability to adopt various conformations, offer significant advantages in the formation of entangled CPs. The reaction between copper sulfate and *N*,*N*′-di(4-pyridyl)adipoamide has been demonstrated to yield a twelve-fold interpenetrated diamondoid network [9]. Entangled CPs, constructed using flexible ligands such as *N*,*N*′-di(4-pyridyl)suberoamide [10] and *N*,*N*′-bis(pyrid-3-ylmethyl)adipoamide [11,12], have highlighted the crucial role that angular dicarboxylate ligands play in determining the degree of interpenetration. In our recent studies, we have shown that the combination of angular dicarboxylate

 doi:10.20944/preprints202408.1890.v1

ligands with flexible *N,N′*-di(4-pyridyl)sebacoamide and *N,N′*-di(4-pyridyl)adipoamide ligands enable these molecules to adapt to the steric demands required for the formation of entangled Co(II) CPs [13].

To compare the roles of angular and flexible bpba ligands in the formation of entangled CPs, we synthesized and reacted the 4,4′-oxybis(*N*-(pyridin-3-yl)benzamide (**L**^{1}), shown in Figure 1(a), and *N,N′*-bis(3-methylpyridyl)adipoamide (**L**^{2}), shown in Figure 1(b), with dicarboxylic acid and various divalent metal salts. This resulted in the formation of $\{[Zn_2(\mathbf{L}^1)(1,4\text{-NDC})_2]\cdot MeOH\}_n$ (1,4-H_2NDC = naphthalene-1,4-dicarboxylic acid), **1**; $\{[Cu(\mathbf{L}^1)(1,4\text{-NDC})(H_2O)]\cdot 3H_2O\}_n$, **2**; $\{[Cd(\mathbf{L}^1)(1,4\text{-NDC})]\cdot 2H_2O\}_n$, **3**; $\{[Co_4(\mathbf{L}^2)_{0.5}(1,4\text{-NDC})_3(H_2O)_3(\mu_3\text{-}OH)_2]\cdot EtOH\cdot 2H_2O\}_n$, **4**; $\{[Zn_2(\mathbf{L}^2)(1,4\text{-NDC})_2]\cdot 2CH_3OH\}_n$, **5**; and $[Cd(\mathbf{L}^2)(adipic)(H_2O)]_n$ (H_2adipic = adipic acid), **6**. Structural comparison of these CPs reveals that the identity of the metal plays a significant role in the formation of entangled CPs when mixed ligands are involved. This report focuses on the synthesis and structural characterization of complexes **1** – **6**, along with an evaluation of their thermal and luminescent properties.

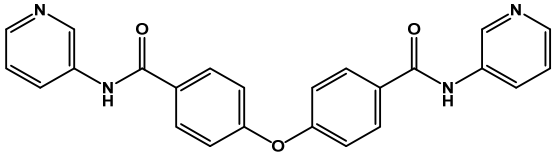

(**a**)

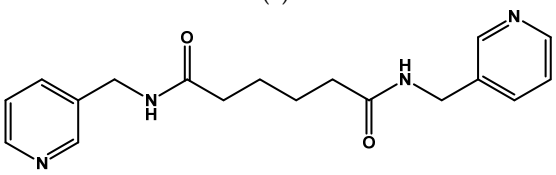

(**b**)

Figure 1. Structures of (a) **L**^{1} and (b) **L**^{2}.

2. Materials and Methods

2.1. General Procedures

Elemental analyses, solid state IR spectra, and powder X-ray diffraction (PXRD) patterns were conducted using a PE 2400 series II CHNS/O analyzer (PerkinElmer Instruments, Shelton, CT, USA), a JASCO FT/IR-460 plus spectrometer (JASCO, Easton, MD, USA), and a Bruker D2 PHASER diffractometer (Bruker Corporation, Karlsruhe, Germany), respectively. Solid-state emission spectroscopy (with excitation and emission slit widths set at 5.0 nm) was performed using a Hitachi F-4500 spectrometer (Hitachi, Tokyo, Japan). Thermogravimetric analysis (TGA) curves were obtained with an SII Nano Technology TGA/DTA 6200 analyzer (Seiko Instruments Inc., Torrance, CA, USA).

2.2. Materials

The reagents zinc acetate dihydrate ($Zn(CH_3COO)_2\cdot 2H_2O$) and copper acetate dihydrate ($Cu(CH_3COO)_2\cdot 2H_2O$) were purchased from SHOWA Co. (Saitama, Japan). Cobalt acetate tetraydrate ($Co(CH_3COO)_2\cdot 4H_2O$), cadmium acetate monohydrate ($Cd(CH_3COO)_2\cdot H_2O$), naphthalene-1,4-dicarboxylic acid (1,4-H_2NDC), and adipic acid (H_2adipic) were sourced from Alfa Aesar (Ward Hill, MA, USA). The ligand 4,4'-oxybis(*N*-(pyridin-3-yl)benzamide (**L**^{1}) [14,15] and *N,N′*-bis(3-methylpyridyl)adipoamide (**L**^{2}) [11] were synthesized following published procedures.

 doi:10.20944/preprints202408.1890.v1

2.3. Preparations

2.3.1. {[$Zn_2(L^1)(1,4\text{-}NDC)_2$]·MeOH}$_n$, **1**

A mixture of $Zn(CH_3COO)_2{\cdot}2H_2O$ (0.022 g, 0.10 mmol), **L**^{1} (0.041 g, 0.10 mmol) and 1,4-H_2NDC (0.022 g, 0.10 mmol) was dissolved in 10 mL of methanol (MeOH) and transferred into a 23 mL Teflon lined stainless steel container. The container was sealed and heated at 100 °C for 48 hours under autogenous pressure, followed by gradual cooling to room temperature. Colorless columnar crystals, suitable for single-crystal X-ray diffraction analysis, were collected, washed with MeOH, and then dried under Vacuum. Yield: 0.024 g (49 %). Anal. calcd for $C_{49}H_{34}N_4O_{12}Zn_2$ (MW = 1001.54): C, 58.76; N, 5.60 ; H, 3.42 %. Found: C, 57.77; N, 5.92; H, 2.69 %. IR (cm^{-1}): 3649(w), 3527(w), 3075(m), 1588(s), 1540(s), 1497(s), 1426(s), 1364(s), 1238(s), 1170(s).

2.3.2. {[$Cu(L^1)(1,4\text{-}NDC)(H_2O)$]·$3H_2O$}$_n$, **2**

The preparation of complex **2** followed a similar procedure to that of complex **1**, with the key difference being the use of a mixture containing $Cu(CH_3COO)_2{\cdot}2H_2O$ (0.02 g, 0.10 mmol), **L**^{1} (0.041 g, 0.10 mmol), and 1,4-H_2NDC (0.022 g, 0.10 mmol) in a solvent mixture of 2 mL of MeOH and 8 mL of water (H_2O). Blue crystals were obtained, which were subsequently washed with MeOH. Yield: 0.099 g (57 %). Anal. calcd for $C_{36}H_{32}CuN_4O_{11}$ (MW = 760.19): C, 56.88; N, 7.37; H, 4.24 %. Found: C, 56.52; N, 7.61; H, 4.21%. IR (cm^{-1}): 3443(s), 3388(s), 1632(s), 1555(s), 1492(s), 1425(s), 1324(s), 1246(s).

2.3.3. {[$Cd(L^1)(1,4\text{-}NDC)$]·$2H_2O$}$_n$, **3**

The synthetic procedure of complex **3** is similar to that of complex **1**, with the exception that a mixture containing $Cd(CH_3COO)_2$ H_2O (0.03 g, 0.10 mmol), **L**^{1} (0.041 g, 0.10 mmol), and 1,4-H_2NDC (0.022 g, 0.10 mmol) in 8 mL of ethanol and 2 mL of H_2O was used. Colorless crystals were obtained, which were then washed with ethanol (EtOH). Yield: 0.057 g (74 %). Anal. calcd for $C_{36}H_{28}CdN_4O_9$ (MW = 773.02): C, 55.93; N, 7.25; H, 3.65 %. Found: C, 54.80; N, 6.97; H, 3.68 %. Anal Calcd for $C_{36}H_{28}CdN_4O_9$ + H_2O (MW = 791.068): C, 54.66; N, 7.08; H, 3.82 %. IR (cm^{-1}): 3554.9(s), 3275.9(s), 1558.8(m), 1550.4(m), 1234.9(s), 1172.9(m), 1071(m), 873.6(s), 744.9(s).

2.3.4. {[$Co_4(L^2)_{0.5}(1,4\text{-}NDC)_3(H_2O)_3(\mu_3\text{-}OH)_2$]·EtOH·$2H_2O$}$_n$, **4**

A 23 mL Teflon-lined steel autoclave was sealed after adding $Co(OAc)_2{\cdot}4H_2O$ (0.025 g, 0.10 mmol), **L**^{2} (0.033 g, 0.10 mmol), 1,4-H_2NDC (0.022 g, 0.10 mmol), 2 mL H_2O and 8 mL ethanol. The autoclave was then heated to 120 °C for two days, followed by slow cooling to room temperature. Purple crystals were formed, which were subsequently collected and purified. Yield: 0.0055 g (18 %). Anal. calcd for $C_{47}H_{47}Co_4N_2O_{21}$ (MW = 1211.58): C, 46.59; N, 2.31; H, 3.91 %. Found: C, 45.91; N, 2.14; H, 3.99 %. FT-IR (cm^{-1}): 3296(m), 1600(s), 1411(s), 1366(s), 785(m).

2.3.5. {[$Zn_2(L^2)(1,4\text{-}NDC)_2$]·$2CH_3OH$}$_n$, **5**

The preparation of complex **5** followed the same procedure as for complex **4**, with the exception that $Zn(OAc)_2{\cdot}2H_2O$ (0.044 g, 0.20 mmol), **L**^{2} (0.098 g, 0.30 mmol), 1,4-H_2NDC (0.043 g, 0.20 mmol) and 10 mL methanol were used. This resulted in the formation of colorless crystals. Yield: 0.080 g (84 %). Anal. calcd for $C_{44}H_{42}N_4O_{12}Zn_2$ + $2H_2O$ (MW = 985.63): C, 53.62; N, 5.68; H 4.70 %. Found: C, 53.89; N, 5.94; H, 4.00 %. FT-IR (cm^{-1}): 3420(s), 1628(m), 1412(m), 1366(m), 828(w), 794(w), 773(w), 700(w), 669(w).

2.3.6. [$Cd(L^2)(adipic)(H_2O)$]$_n$, **6**

The synthesis of complex **6** mirrored that of complex **4**, with the exception that $Cd(OAc)_2{\cdot}2H_2O$ (0.027 g, 0.10 mmol), **L**^{2} (0.033 g, 0.10 mmol), and adipic acid (0.015 g, 0.10 mmol) were used in a solvent mixture of 8 mL H_2O and 2 mL ethanol. This process yielded colorless crystals. Yield: 0.012 g

 doi:10.20944/preprints202408.1890.v1

(21 %). Anal. calcd for $C_{24}H_{32}CdN_4O_7$ (MW = 600.93): C, 47.97; N,9.32; H, 5.37 %. Found: C, 47.61; N, 9.05; H, 5.49 %. FT-IR (cm^{-1}): 3415(s), 3262(s), 1643(s), 1542(s), 2922(m), 1306(w), 647(w).

The phase purities of complexes **1** – **6** were confirmed using powder X-ray diffraction (PXRD). As illustrated in Figures S1 – S6, the experimental PXRD patterns closely match the corresponding simulated ones, indicating the bulk purity of complexes **1** – **6**.

2.4. X-ray Crystallography

The diffraction data for complexes **1–6** were collected using a Bruker AXS SMART APEX II CCD diffractometer with graphite-monochromated MoK (α = 0.71073 Å). Data reduction, including Lorentz and polarization corrections as well as an empirical absorption correction based on the multi-scan method, was performed using established computational procedures [16]. The positions of the heavier atoms were determined using the Pattern or direct methods, while the remaining atoms were located through successive difference Fourier maps and least-square refinements. Hydrogen atoms, except those in water molecules, were add using the HADD command in SHELXTL 6.1012 [17]. The crystal data for complexes **1-6** are summarized in Table 1.

Table 1. Crystal data for complexes **1–6**.

	1	**2**	**3**
Formula	$C_{49}H_{34}N_4O_{12}Zn_2$	$C_{36}H_{32}CuN_4O_{11}$	$C_{36}H_{28}CdN_4O_9$
Formula weight	1001.54	760.19	773.02
crystal system	Monoclinic	Orthorhombic	Monoclinic
space group	*C*2/*c*	$P2_12_12_1$	*C*2/*c*
a, Å	16.4613(4)	10.8657(4)	29.3869(4)
b, Å	14.2488(3)	16.0134(5)	10.0253(1)
c, Å	20.9984(5)	19.2892(7)	21.6458(3)
α,°	90	90	90
β,°	105.7361(13)	90	93.1008(7)
γ,°	90	90	90
V, $Å^3$	4740.66(19)	3356.3(2)	6367.79(14)
Z	4	4	8
d_{calc}, mg/m^3	1.403	1.504	1.613
F(000)	2048	1572	3136
μ(MoKα), mm^{-1}	1.078	0.721	0.752
range(2θ) for data collection,deg	3.84 ≤ 2θ ≤ 52.00	3.30 ≤ 2θ ≤ 56.64	2.77 ≤ 2θ ≤ 56.61
independent reflections	4678 [R(int) = 0.0368]	8348 [R(int) = 0.0342]	7862 [R(int) = 0.0247]
data/restraints/parameters	4678 / 1 / 319	8348 / 0 / 470	7862 / 1 / 451
quality-of-fit indicator [c]	1.010	1.017	1.060
final R indices [I > 2σ(I)] [a,b]	R1 = 0.0602, wR2 = 0.1417	R1 = 0.0377, wR2 = 0.0841	R1 = 0.0292, wR2 = 0.0705
R indices (all data)	R1 = 0.0635, wR2 = 0.1429	R1 = 0.0526, wR2 = 0.0904	R1 = 0.0370, wR2 = 0.0746

[a] $R_1 = \Sigma \| F_o | - | F_c \| / \Sigma | F_o |$. [b] $wR_2 = [\Sigma w(F_o^2 - F_c^2)^2 / \Sigma w(F_o^2)^2]^{1/2}$. $w = 1/[\sigma^2(F_o^2) + (ap)^2 + (bp)]$, $p = [\max(F_o^2 \text{ or } 0) + 2(F_c^2)]/3$. a = 0, b = 75.1500 for **1**; a = 0.0427, b = 1.2489 for **2**; a = 0.0321, b = 9.5066 for **3**; a = 0.1155, b = 6.7541 for **4**; a = 0.0436, b = 6.4686 for **5**; a = 0.0264, b = 0.0592 for **6**. [c] quality-of-fit = $[\Sigma w(|F_o^2| - |F_c^2|)^2/(N_{observed} - N_{parameters})]^{1/2}$.

 doi:10.20944/preprints202408.1890.v1

Table 1. Crystal data for complexes 1–6. (cont.).

	4	**5**	**6**
Formula	$C_{47}H_{47}Co_4N_2O_{21}$	$C_{44}H_{42}N_4O_{12}Zn_2$	$C_{24}H_{32}CdN_4O_7$
Formula weight	1211.58	949.55	600.93
crystal system	Monoclinic	Monoclinic	Monoclinic
space group	$P2_1/c$	$P2_1/c$	$C2/c$
a, Å	11.5475(13)	18.5332(3)	19.7055(7)
b, Å	21.944(2)	15.1797(3)	15.5586(6)
c, Å	20.800(2)	15.6862(3)	8.7536(3)
α,°	90	90	90
β,°	92.035(2)	107.0289(10)	111.408(2)
γ,°	90	90	90
V, Å^3	5267.1(10)	4219.50(14)	2498.60(16)
Z	4	4	4
d_{calc}, mg/m^3	1.528	1.495	1.597
F(000)	2476	1960	1232
μ(Mo Kα), mm^{-1}	1.316	1.206	0.926
range(2θ) for data collection,deg	3.53 ≤ 2θ ≤ 52.00	3.53 ≤ 2θ ≤ 52.00	3.43 ≤ 2θ ≤ 56.57
independent reflections	10343	8290	3091
	[R(int) = 0.1108]	[R(int) = 0.0528]	[R(int) = 0.0608]
data/restraints/parameters	10343 / 1101 / 649	8290 / 2 / 549	3091 / 0 / 168
quality-of-fit indicator [c]	1.051	1.013	1.018
final R indices [I > 2σ(I)] [a,b]	R1 = 0.0766, wR2 = 0.1945	R1 = 0.0475, wR2 = 0.1033	R1 = 0.0401, wR2 = 0.0670
R indices (all data)	R1 = 0.1500, wR2 = 0.2315	R1 = 0.1029, wR2 = 0.1240	R1 = 0.0728, wR2 = 0.0758

3. Results

*3.1. Structure of **1***

Single-crystal X-ray crystallographic analysis reveals that complex **1** crystallizes in the monoclinic space group *C*2/*c*, with each asymmetric unit containing two Zn(II) ion, one **L**^{1} ligand, two 1,4-NDC^{2-} ligands and one coordinated MeOH molecule. Figure 2(a) depicts the coordination environment surrounding the dinuclear Zn(II) metal centers [Zn---Zn = 3.0037(10) Å]. Each of the symmetry-related Zn(II) ions is five-coordinated by one pyridyl nitrogen atom [Zn-N = 2.034(4) Å] from the **L**^{1} ligand and four carboxylate oxygen atoms [Zn-O = 1.993(4) - 2.09(5) Å] from four 1,4-NDC^{2-} ligands, resulting in distorted square pyramidal geometries (τ_5 = 0.20; τ_5 = 1 and 0 indicate trigonal bipyramidal and square pyramidal geometries, respectively) [18]. The dinuclear paddle-wheel Zn(II) units are further extended through the connection of **L**^{1} and 1,4-NDC^{2-} ligands to form a three-dimensional (3D) framework. Topologically, if the Zn(II) ions are considered as six-connection nodes, the 1,4-NDC^{2-} ligands as four-connected nodes, and the **L**^{1} ligands as linkers, the structure of **1** can be simplified as a 3D framework with the rare $(3^2.6^2.7^2)(3^4.4^6.6^4.7)$-sqc493 topology (standard representation) [19], as depicted in Figure 2(b), showing 2-fold interpenetration, illustrated in Figure 2(c). Furthermore, if the dinuclear units are treated as 6-connected nodes, with **L**^{1} and 1,4-NDC^{2-} ligands serving as linkers, the structure of **1** can be simplified as a 6-connected, 2-fold interpenetrated 3D net with the $(4^{12}.6^3)$-**pcu** topology, as shown in Figures 2(d) and 2(e).

 doi:10.20944/preprints202408.1890.v1

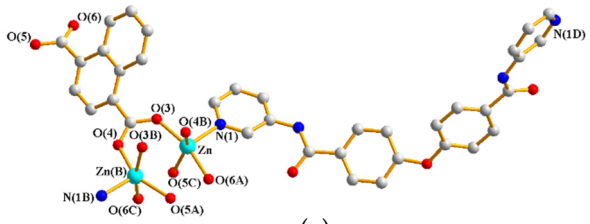

(**a**)

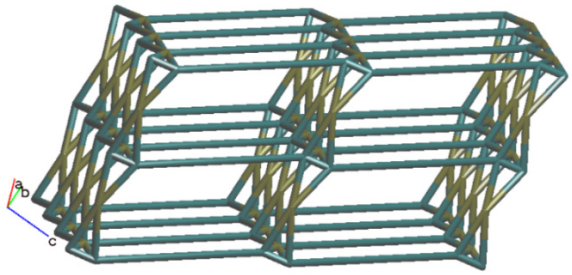

(**b**)

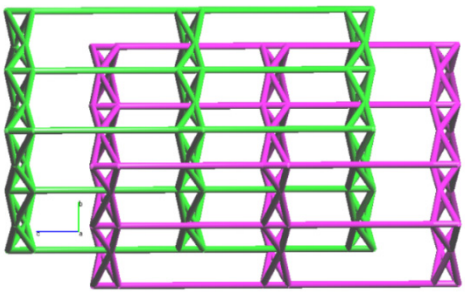

(**c**)

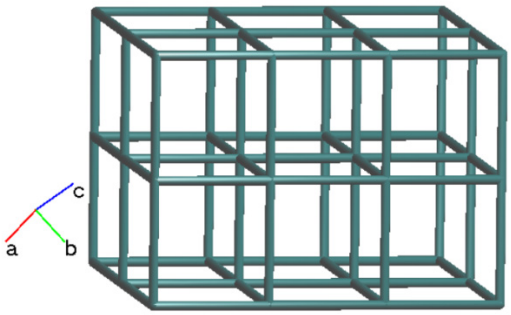

(**d**)

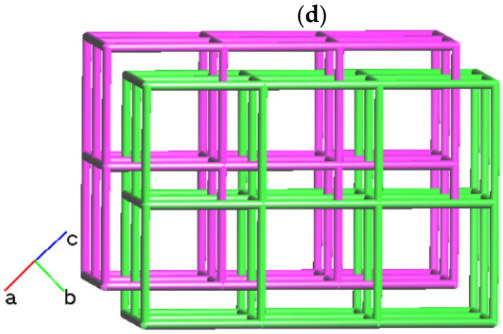

(**e**)

Figure 2. (**a**) Coordination environments about the Zn(II) ions. Symmetry transformations used to generate equivalent atoms: (A) x + 1/2, y + 1/2, z; (B) -x + 1, y, -z + 3/2; (C) -x + 1/2, y + 1/2, -z + 3/2. (**b**) A drawing showing the 3D framework with the sqc493 topology. (**c**) A drawing showing the 2-fold interpenetrated 3D framework with the sqc493 topology. (**d**) A drawing showing the 3D framework with the **pcu** topology. (**e**) A drawing showing the 2-fold interpenetrated 3D framework with the **pcu** topology.

 doi:10.20944/preprints202408.1890.v1

3.2. Structure of **2**

Crystals of complex **2** conform to the orthorhombic noncentrosymmetric space group $P2_12_12_1$, with each asymmetric unit containing one Cu(II) ion, one $\mathbf{L}^1$ ligand, one 1,4-NDC^{2-} ligand, one coordinated water molecule, and three cocrystallized water molecules. Figure 3(a) illustrates the coordination environment around the Cu(II) metal center, which is five-coordinated by two pyridyl nitrogen atoms [Cu-N = 2.075(3) and 2.077(2) Å] from two $\mathbf{L}^1$ ligands, two carboxylate oxygen atoms [Cu-O = 1.962(2) – 1.973(2) Å] from two 1,4-NDC^{2-} ligands, and one oxygen atom [Cu-O = 2.346(3) Å] from the coordinated water molecule, resulting in a square pyramidal geometry (τ_5 = 0.01). Through the linkage provided by the $\mathbf{L}^1$ ligands, the Cu(II) ions are arranged into a one-dimensional (1D) 2-fold $[Cu\mathbf{L}^1]_n$ helix with a pitch of 17.31 Å. Notably, the angular backbones of the $\mathbf{L}^1$ ligands enable the interleaving of two additional helices, resulting in a fascinating triple-stranded helix within the structure of complex **2**, as shown in Figure 3(b). The triple-stranded helices are further stabilized by linear chains formed by the 1,4-NDC^{2-} ligands, resulting in the formation of a 1D single-walled nanotubular framework, as depicted in Figure 3(c).

The triple-stranded structure of complex **2** stands in marked contrast to the quadruple-stranded structure of $[Co(\mathbf{L}^3)(2,4\text{-PDC})(H_2O)]_n$ [where $\mathbf{L}^3$ = *N,N′*-di(3-pyridyl)suberoamide and 2,4-H_2PDC = 2,4-pyridinedicarboxylic acid) [20], as well as the quintuple-stranded structure of $[Zn(2,4\text{-PDC})(\mathbf{L}^4)(H_2O)]_\infty$ (where $\mathbf{L}^4$ = *N,N′*-di(3-pyridyl)dodecanediamide) [21]. This observation suggests that the number of helices is likely influenced by the combined effects of the metal and ligand identities.

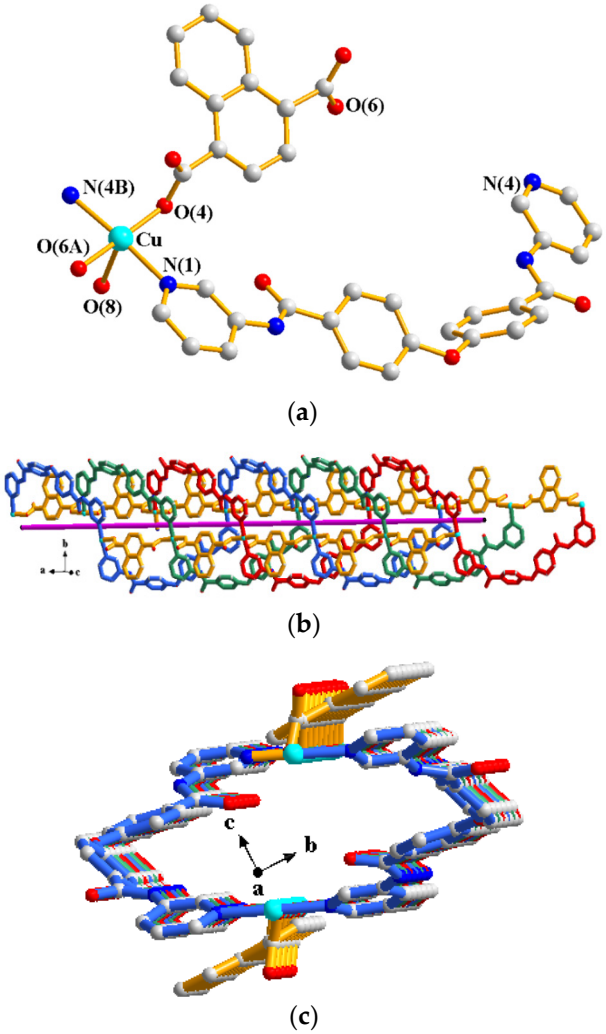

Figure 3. (**a**) Coordination environments about the Cu(II) ion. Symmetry transformations used to generate equivalent atoms: (A) x - 1, y, z; (B) x - 3/2, -y + 3/2, -z + 2. (**b**) A drawing showing the triple-strained helix. (**c**) Another view looking down the *a*-axis.

 doi:10.20944/preprints202408.1890.v1

3.3. Structure of ***3***

The structure of complex **3** was solved in the monoclinic space group *C*2/*c*, with each asymmetric unit containing one Cd(II) ion, one $\mathbf{L}^1$ ligand, one 1,4-NDC^{2-} ligand, and two co-crystallized water molecules. Figure 4(a) illustrates the coordination environments around the dinuclear Cd(II) metal centers. Each of the symmetry-related Cd(II) ions is six-coordinated by two pyridyl nitrogen atoms [Cd-N = 2.3642(19) and 2.3473(18) Å] from two $\mathbf{L}^1$ ligands and four carboxylate oxygen atoms [Cd-O = 2.3053(14) - 2.4408(15) Å] from three 1,4-NDC^{2-} ligands, resulting in distorted octahedral geometries. Topologically, when considering the Cd(II) ions as four-connection nodes and the 1,4-NDC^{2-} ligands as three-connection nodes, with the $\mathbf{L}^1$ ligands acting as linkers, the structure of complex **3** can be simplified into a 3D network with a $(4^2.6.10^2.12)(4^2.6)$-**coe**-3,4-C2/c topology, Figure 4(b), exhibiting a 3-fold interpenetration (standard representation), as seen in Figure 4(c). Furthermore, when the dinuclear units are considered as 4-connected nodes, and the $\mathbf{L}^1$ and 1,4-NDC^{2-} ligands as linkers, the structure of complex **3** can be further simplified into a 3-fold interpenetrated 3D network with a (6^6)-**dia** topology (cluster representation), as depicted in Figures 4(d) and 4(e).

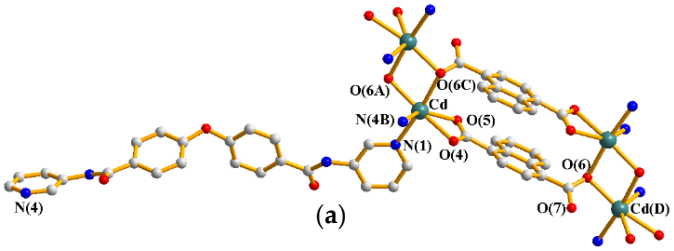

(**a**)

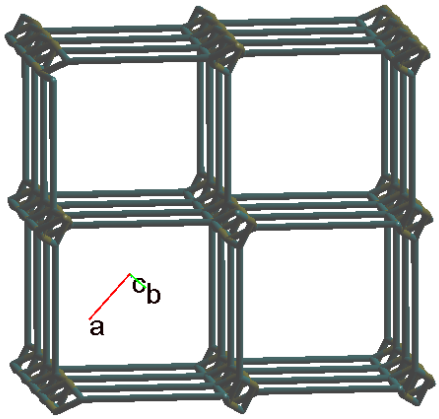

(**b**)

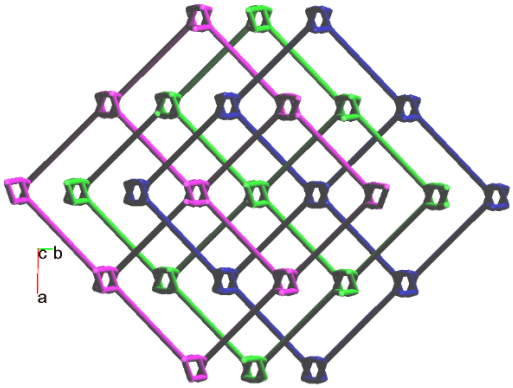

(**c**)

 doi:10.20944/preprints202408.1890.v1

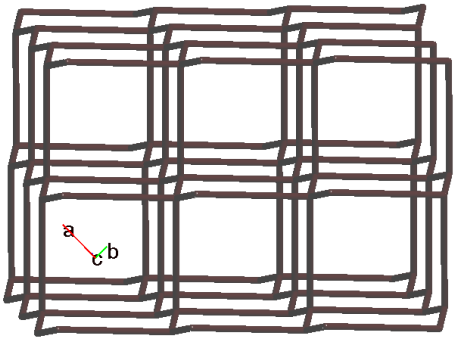

(**d**)

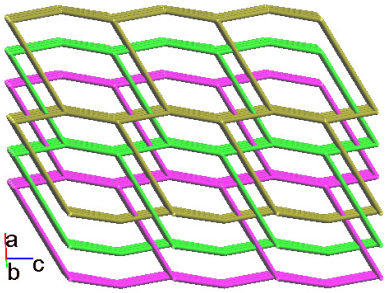

(**e**)

Figure 5. (**a**) Coordination environments about the Cd(II) ions. Symmetry transformations used to generate equivalent atoms: (A) x, -y + 2, z - 1/2; (B) -x + 1/2, -y + 1/2, -z; (C) -x, -y + 2, -z + 1; (D) x, -y + 2, z + 1/2. (**b**) A drawing showing the 3D framework with the **coe** topology. (**c**) A drawing showing the 3-fold interpenetrated 3D framework with the **coe** topology. (**d**) A drawing showing the 3D framework with the **dia** topology. (**e**) A drawing showing the 3-fold interpenetrated 3D framework with the **dia** topology.

*3.4. Structure of **4***

Complex **4** crystallizes in the monoclinic space group $P2_1/c$, with each asymmetric unit comprising four Co(II) ions, a half of an **L**^{2} ligand positioned at independent inversion centers, three 1,4-NDC^{2-} ligands, two μ_3-OH$^-$ groups, three coordinated water molecules, and two co-crystallized water molecules, as shown in Figure 5(a). Figure 5(b) illustrates the coordination environment around the Co(II) metal centers, where Co(1), Co(2) and Co(3) atoms exhibit distorted octahedral geometries, while Co(4) displays a distorted square pyramidal geometry (τ_5 = 0.43). The Co(1) atom is coordinated by six oxygen atoms from four 1,4-NDC^{2-} ligands [Co-O = 2.055(5) - 2.161(5) Å], one OH$^-$ group [Co-O = 2.110(4) Å] and one coordinated water molecule [Co-O = 2.068(4) Å]. The Co(2) atom is coordinated by six oxygen atoms from three 1,4-NDC^{2-} ligands [Co-O = 2.068(5) - 2.134(4) Å], two OH$^-$ groups [Co-O = 2.111(4) - 2.131(4) Å] and one coordinated water molecule [Co-O = 2.075(4) Å]. In contrast, the Co(3) atom is coordinated by one nitrogen atom from the **L**^{2} ligand [Co-N = 2.095(5) Å] and five oxygen atoms from three 1,4-NDC^{2-} ligands [Co-O = 2.086(5) - 2.189(4) Å], one OH$^-$ group [Co-O = 2.092(4) Å] and one coordinated water molecule [Co-O = 2.095(5) Å]. Lastly, the Co(4) atom is coordinated by five oxygen atoms from three 1,4-NDC^{2-} ligands [Co-O = 2.025(4) - 2.130(5) Å] and two OH$^-$ groups [Co-O = 1.984(4) - 2.019(4) Å]. Additionally, two symmetry-related Co_4(1,4-NDC)$_3$(**L**)$_{0.5}$(H_2O)$_3$(μ_3-OH)$_2$ units are linked together to form a Co_8 cluster, which are further interconnected by **L**^{2} and 1,4-NDC^{2-} ligands to create a 3D framework.

Topologically, the Co(II) ions can be regarded as five connected nodes, the 1,4-NDC^{2-} ligands as four- and five-connected nodes and the μ_3-OH ligands as three connected-nodes, with the **L**^{2} ligands acting as linkers. This arrangement results in a 3D framework with a $(4^2{\cdot}6{\cdot}8^3)(4^2{\cdot}6^2{\cdot}7{\cdot}8)(4^2{\cdot}6)_2(4^3{\cdot}6{\cdot}7^2{\cdot}8^4)(4^4{\cdot}6^4{\cdot}7{\cdot}8)(4^4{\cdot}7{\cdot}8^4{\cdot}9)(4^6{\cdot}6^4)_2$-3,3,4,4,5,5,5,5,5T1 topology, Figure 5(c).

 doi:10.20944/preprints202408.1890.v1

Furthermore, if the Co_8 clusters are considered as eight-connected nodes, the structure of complex **4** can be simplified into a uninodal self-penetrating network with a $(4^{20}\cdot6^8)$-8T32 topology, as shown in Figure 5(d). For comparison, a similar coordination polymer with mixed ligands, having the formula $\{[Co_8(\mu_3\text{–}OH)_4(1,4\text{-NDC})_6(btp)(H_2O)_6]\cdot H_2O\}_n$ [btp = 4,4′-bis(triazol-1-ylmethyl)biphenyl)] has been reported [22].

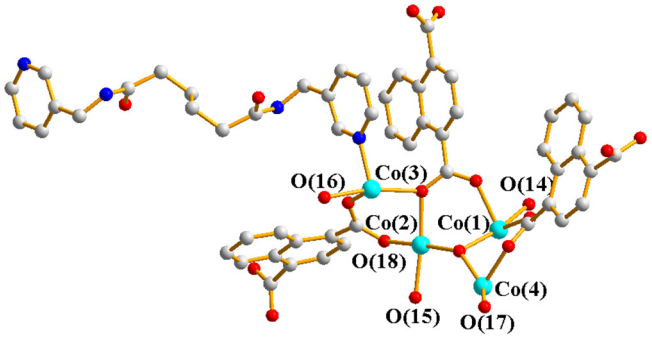

(a)

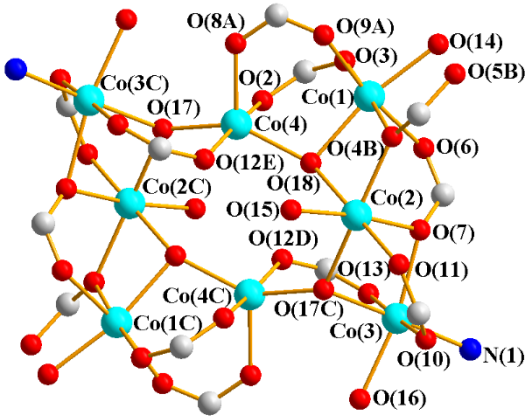

(b)

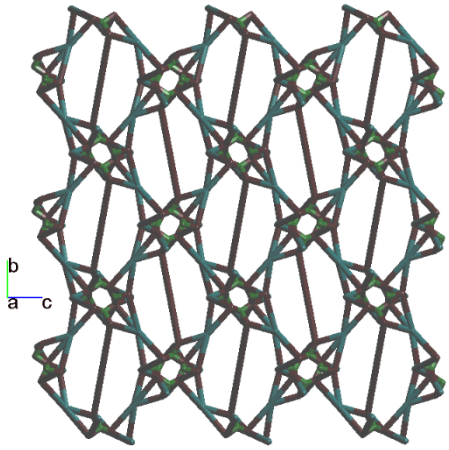

(c)

Preprints.org (www.preprints.org) | NOT PEER-REVIEWED | Posted: 27 August 2024 doi:10.20944/preprints202408.1890.v1

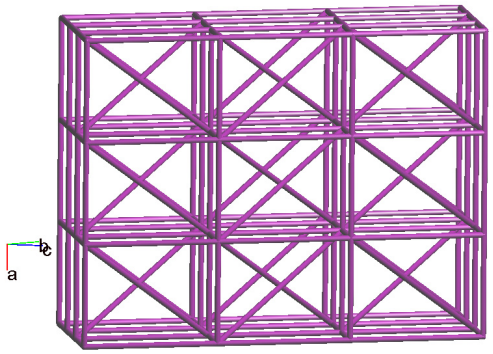

(d)

Figure 6. (**a**) A drawing showing the asymmetric unit of **4**, except the cocrystallized water molecules, with full **L²** ligand that occupies an inversion center. The **L²** and 1,4-NDC^{2-} ligands are not labeled for clarity. (**b**) Coordination environments about the Co(II) ions of the octanuclear cluster of **4**. The **L²** ligands and the 1,4-NDC^{2-} ligands are represented by the are represented by the N atoms and the OCO groups, respectively. Symmetry transformations used to generate equivalent atoms: (A) –x + 2, y - 1/2, -z + 1/2; (B) x - 1, y, z; (C) –x + 2, -y + 2, -z + 1; (D) x + 1, y, z ; (E) –x + 1, -y + 2, -z + 1. (**c**) A drawing showing the 3D framework with the 3,3,4,4,5,5,5,5T1 topology. (**d**) A drawing showing the self-catenated 3D framework with the (4^{20}·6^{8})-8T32 topology.

3.5. Structure of ***5***

Crystal structure of complex **5** was resolved in the monoclinic space group $P2_1/c$. Each asymmetric unit contains two Zn(II) ions, one **L²** ligand, two 1,4-NDC^{2-} ligands and two co-crystallized methanol molecules. Figure 6(a) illustrates the coordination environment around the Zn(II) metal centers, revealing that Zn(1) (τ_5 = 0.11) and Zn(2) (τ_5 = 0.11) atoms adopt distorted square pyramidal geometries. The Zn(1) and Zn(2) atoms are each coordinated by four oxygen atoms from four 1,4-NDC^{2-} ligands [Zn(1)-O = 2.039(3) – 2.064(3) Å; Zn(2)-O = 2.026(3) – 2.072(3) Å] and one nitrogen atom from the **L²** ligand [Zn(1)-N(1) = 2.018(3) Å; Zn(2)-N(4C) = 2.026(3) Å]. The two Zn(II) ions are bridged by four 1,4-NDC^{2-} ligands in a paddlewheel fashion, which are further axially linked by the **L²** ligands to form two-dimensional (2D) layers. Topologically, when considering the Zn(II) ions as five-connected nodes, the 1,4-NDC^{2-} ligands as four-connected nodes, and the **L²** ligands as linkers, the structure of complex **5** can be simplified to a 4,5-coordinated 2D network with the new (4^2·6^3·8)(4^6·6^4) topology (standard representation), as shown in Figure 6(b). Alternatively, If the dinuclear units are regarded as four-connected nodes and the organic ligands as linkers, the structure of complex **5** can be further simplified to a six-connected 2D net with the (4^{13}·6^2)-(4,4)IIb topology (cluster representation), as depicted in Figure 6(c).

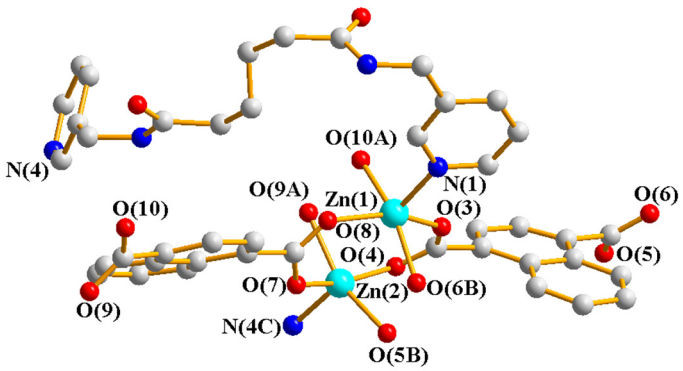

(a)

 doi:10.20944/preprints202408.1890.v1

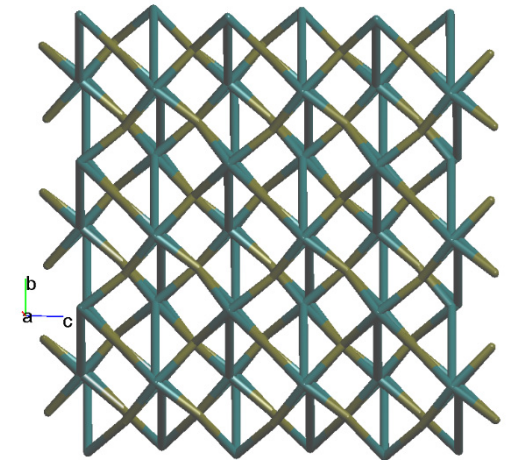

(**b**)

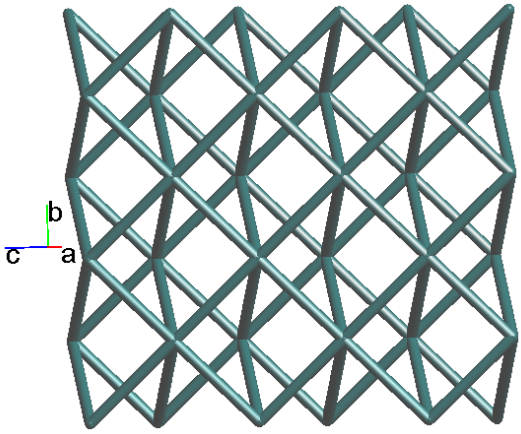

(c)

Figure 6. (**a**) Coordination environments about the Zn(II) ions of the octanuclear cluster of **5**. Symmetry transformations used to generate equivalent atoms: (A) x, -y + 1/2, z + 1/2 ; (B) x, -y + 3/2, z - 1/2; (C) –x + 1, y + 1/2, -z + 1/2. (**b**) A drawing showing the 2D net with the $(4^2{\cdot}6^3{\cdot}8)(4^6{\cdot}6^4)$ topology. (**c**) A drawing showing the 2D net with the $(4^{13}{\cdot}6^2)$-(4,4)IIb topology.

3.6. Structure of ***6***

Crystals of complex **6** conform to the monoclinic space group *C*2/*c*, with each asymmetric unit containing a half of a Cd(II) ion, half of an **L²** ligand, half of an adipic^{2-} ligand, and half of a coordinated water molecule. Figure 7(a) illustrates the coordination environment around the Cd(II) metal center. The Cd atom is coordinated by four oxygen atoms from two adipic^{2-} ligands [Cd-O = 2.384(2) and 2.457(2) Å], two nitrogen atoms from two **L** ligands [Cd-N = 2.344(2)] and one oxygen atom from the water molecule [Cd-O(4) = 2.320(4) Å], resulting in a distorted pentagonal bipyramidal geometry. The Cd(II) ions are bridged by the **L²** and adipic^{2-} ligands, forming pairs of 2D layers, Figure 7(b), that interdigitate with each other through water molecules, as shown in Figure 7(c) and Figure 7(d). Topologically, if the Cd ions are considered four-connected nodes, and the organic ligands as linkers, the structure of complex **6** can be further simplified into a four-coordinated 2D network with a $(4^4{\cdot}6^2)$-**sql** topology, as depicted in Figure 7(e).

 doi:10.20944/preprints202408.1890.v1

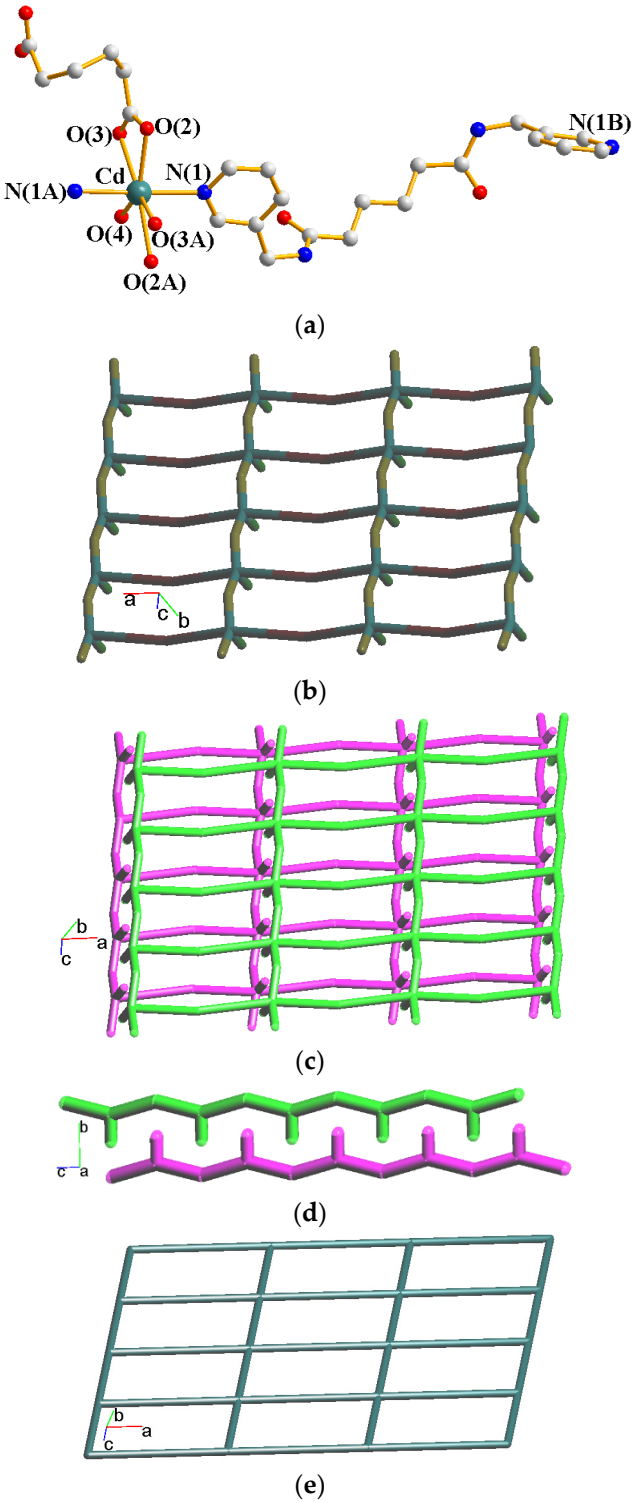

(**a**)

(**b**)

(**c**)

(**d**)

(**e**)

Figure 7. (**a**) Coordination environments about the Cd(II) ion of **6**. Symmetry transformations used to generate equivalent atoms: (A) –x + 1, y, -z + 3/2 ; (B) –x + 2, y, -z + 3/2. (**b**) A simplified drawing showing that the Cd(II) ions, which are coordinated by the water molecules, are bridged by the $\mathbf{L}^2$ and adipic^{2-} ligands to form a 2D layer. (**c**) and (**d**) Two different views showing the arrangement of a pair of the 2D layers. (**e**) A drawing showing the simplified 2D net with the $(4^4{\cdot}6^2)$-**sql** topology.

The combination of the angular $\mathbf{L}^1$ or flexible $\mathbf{L}^2$ with the rigid, linear dicarboxylate 1,4-NDC^{2-} resulted in the formation of interpenetrated CPs **1** and **3**, as well as a self-catenated 3D framework in complex **4**. In a previous study, we proposed that Co(II) CPs supported by the angular dicarboxylate ligand and the flexible bpba ligand, can be adjusted to meet the steric requirements necessary for the

 doi:10.20944/preprints202408.1890.v1

formation of the entangled networks [14]. The fact that complexes **1**, **3** and **4** exhibit entangled structures, while the other two do not, suggests that the identity of the metal ion plays a crucial role. When supported by 1,4-NDC^{2-}, the angular $\mathbf{L^1}$ may form the entangled networks if the appropriate metal ion is used. Conversely, the combination of 1,4-NDC^{2-} with flexible bpba ligands led to the formation of non-entangled Cd(II) CPs, including $\{[Cd(\mathbf{L^2})(1,4\text{-}NDC)(H_2O)]\cdot H_2O\}_n$, $\{[Cd(L^A)(1,4\text{-}NDC)]\cdot 2H_2O\}_n$ [L^A = bis(N-pyrid-3-ylmethyl)suberoamide], and $\{[Cd_2(L^A)(1,4\text{-}NDC)_2]\cdot 3H_2O\}_n$. These structures exhibit a 2D layer with the $(4^4\cdot6^2)$-**sql** topology and 3D frameworks with the $(3^2\cdot6^2\cdot7^2)(3^2\cdot6^5\cdot7^3)_2$-4,5T61 and $(3^2\cdot5^4)(3^4\cdot4^6\cdot5^8\cdot6^6\cdot7^4)$-sqc776 topologies, respectively [23]. Interestingly, a structural comparison of complex **6** with $\{[Cd(\mathbf{L^2})(1,4\text{-}NDC)(H_2O)]\cdot H_2O\}_n$, which shares the same structural topology, indicate that the Cd(II) ion is a key factor in determining the structural type.

3.7. Ligand Conformation and Bonding Mode

The conformations of the bpba ligands are defined as follows: If the torsional angle (θ) of the bridging carbon atoms is within the range of $0 \le \theta \le 90^o$, the confirmation is classified as gauche (G); if $90 < \theta \le 180^o$, it is classified as anti (A). Additionally, the terms *cis* and *trans* are used to describe whether the two C=O groups are oriented in the same direction (*cis*) or in the opposite direction (*trans*). Due to varying orientations of the pyridyl nitrogen atoms and the amide oxygen atoms, three additional conformations: *syn-syn*, *syn-anti* and *anti-anti*, can also be observed for bpba ligands. In this context, the $\mathbf{L^1}$ ligands in complex **1** adopt *cis syn-syn* confirmation, while in complexes **2** and **3**, they adopt the *trans syn-anti* confirmation. The $\mathbf{L^2}$ ligands in complexes **4**, **5**, and **6** exhibit the following confirmations, respectively: GAG *trans anti-anti*, GAG *cis anti-anti*, and AAA *trans syn-syn* (see Table 2 for details). Furthermore, the dicarboxylate ligands in complexes **1** – **6** bridge between two to five metal ions, resulting in diverse coordination modes. Notably the 1,4-NDC^{2-}ligands in complex **4** adopt three different coordination modes, leading to the formation of a self-catenated 3D framework.

Table 2. Ligand conformations of $\mathbf{L^1}$ and $\mathbf{L^2}$ and coordination modes of dicarboxylate ligands in **1** – **6**.

	Ligand conformation	Coordination mode
1	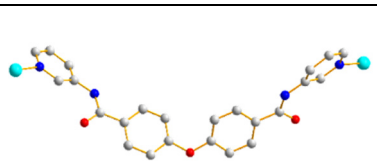	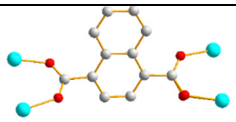
	cis syn-syn	μ_4-O:κO′:κO′′:κO′′′
2	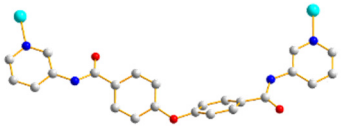	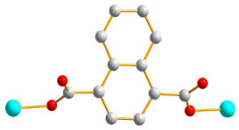
	trans syn-anti	μ_2-κO: κO′
3	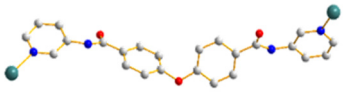	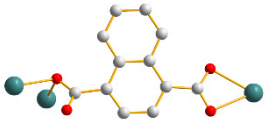
	trans syn-anti	μ_3-κ^2O′O′′:κO:κO

 doi:10.20944/preprints202408.1890.v1

4	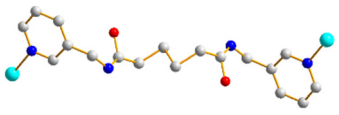 GAG *trans anti-anti*	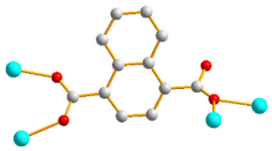 μ_4-κO:κO′:κO′′:κO′′	
		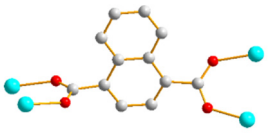 μ_4-κO:κO′:κO′′:κO′′′	
		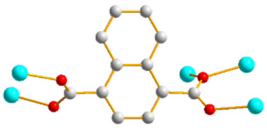 μ_5-κO:κO′:κO′′:κO′′:κO′′′	
5	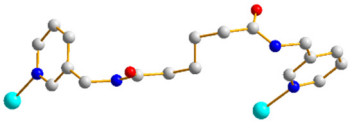 GAG *cis anti-anti*	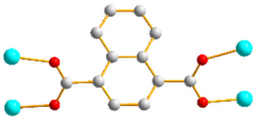 μ_4-κO:κO′:κO′′:κO′′′	
6	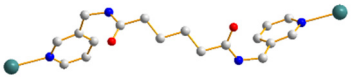 AAA *trans syn-syn*	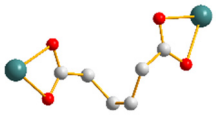 μ_4-κ²O,O′:κ²O′′,O′′′	

The structural differences in **L**¹ ligands of complexes **1** – **3** can be further analyzed. As illustrate in Figure 8, distances d1 and d2 represent the distances from the bridging oxygen atom to the two metal ions, while d3 is the distance between the two metal ions bridged by the **L**¹ ligand. Additionally, θ1, θ2, and θ3 refer to the dihedral angles between the adjacent six-membered rings, specifically the angles between rings I and II, II and III, and III and IV, respectively. The C-O-C angle represents the bond angle around the bridging oxygen atom. Table 3 shows that the distances d1, d2 and d3, as well as the C-O-C angles are similar across complexes **1** – **3**. However, the θ1, θ2, and θ3 angles exhibit significant variations, highlighting the influence of the metal ions on the structural configuration of the **L**¹ ligand. These differences contribute to the distinct structural types observed in complexes **1** – **3**.

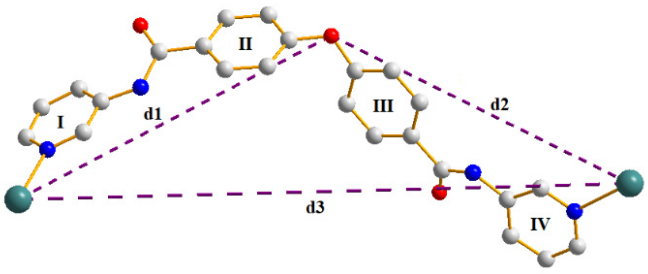

Figure 8. A schematic diagram defining the distances and the dihedral angle.

 doi:10.20944/preprints202408.1890.v1

Table 3. Comparison of angles and distance for Complexes **1 - 3**.

complex	d1 (Å)	d2 (Å)	d3 (Å)	θ1 (°)	θ2 (°)	θ3 (°)	C-O-C
1	11.24	11.24	20.29	41.67	51.07	41.67	123.18
2	11.17	11.39	17.31	52.23	59.04	13.89	121.16
3	11.10	11.43	21.55	77.93	27.74	16.66	121.09

3.8. Structural comparisons

Reactions of divalent metal salts with 4,4′-oxybis(N-(pyridine-4-yl)-benzamide, **L**^{3}, an isomer of **L**^{1}, and 1,4-H_2NDC in various solvents resulted in the formation of [Zn(**L**^{3})(1,4-NDC)·H_2O]$_n$, [Cd(**L**^{3})(1,4-NDC)(H_2O)·MeOH]$_n$, and [Co(**L**^{3})(1,4-NDC)(H_2O)0.5·MeOH]$_n$, all of which exhibit eight-fold interpenetrating frameworks with the **dia** topology [24]. Structural comparisons between these three **L**^{3}-based CPs and the **L**^{1}-based CPs **1** – **3** reveal that the isomerism of **L**^{1} and **L**^{3} plays distinct roles in determining structural diversity. While **L**^{3} primarily governs the structural diversity of the resulting CPs, the structures of CPs containing **L**^{1} are more influenced by the identity of the metal ion. Table 4 summarizes the structures of complexes containing **L**^{1} or **L**^{3} ligands, highlighting the importance of the combined effects of metal and ligand identities, as well as the nature of the solvent molecules, in determining structural diversity. Notably, while entangled CPs are commonly found in **L**^{3}-based CPs, complexes **1** and **3** are unique examples of entangled CPs among those based on **L**^{1}.

Table 4. The structures of metal complexes containing **L**^{1} or **L**^{3}.

Complex	Structure	Reference
[{Cu_2(**L**^{1})(adman)$_4$}·3DMF]$_2$	Dinuclear complex	16
{[Cd(**L**^{1})(5-NIP)(H_2O)]·H_2O}$_n$	2D, **sql**	25
{[Cd(**L**^{1})(2,5-TPD)]·DMA}$_n$	2D, (4^2·6^7·8)(4^2·6)	25
{[Cd(**L**^{1})(2,5-TPD)]·2H_2O}$_n$	2D, (4^2·6^7·8)(4^2·6)	25
{[Zn(**L**^{1})(2,5-TPD)]·2H_2O}$_n$	2D, {4^2·6^2}	25
{[Zn(**L**^{1})(1,3-BDC)]·H_2O}$_n$	2D, {4^2·6^2}	25
{[Zn_2(**L**^{1})(5-AIP)$_2$]·2H_2O}$_n$	2D, {6^3}{6^6}	25
[{Cd(**L**^{1})(IPA)}(H_2O)$_2$]$_n$	2D, {4^2·6^7·8}{4^2·6}	14
[{Cd(**L**^{1})(TPA)}(H_2O)]$_n$	2D, **sql**	14
[{Cd(**L**^{1})$_2$(1,4-PDA)$_2$(H_2O)$_2$}(H_2O)$_6$]$_n$	1D, {4^2.6}	14
[{Cd_2(**L**^{1})$_2$(1,2-CTA)$_2$}(H_2O)$_4$]$_n$	2D, {3^3·4^{10}·5·6}	14
{[Co(**L**^{1})(chdc)]}$_n$	1D wave-like double chain	26
{[Zn(**L**^{1})(hip)]·2.8H_2O}$_n$	2D, **sql**	26
{[Zn_2(**L**^{1})(chdc)$_2$]·2H_2O}$_n$	2D, (4^2·6^3·8)(4^2·6)	27
{[Zn(**L**^{1})(mip)]·3H_2O}$_n$	2D, **sql**	27
{[Zn(**L**^{1})(1,3-BDC)]·H_2O}$_n$	2D, **sql**	27
{[Cd_2(**L**^{1})(chdc)$_2$]·2H_2O}$_n$	2D, (4^2·6^3·8)(4^2·6)	27
{[Cd(**L**^{1})(mip)]·2H_2O}$_n$	2D, (4^2·6^7·8)(4^2·6)	27
{[Cd(**L**^{1})(1,3-BDC)]·2H_2O}$_n$	2D, (4^2·6^7·8)(4^2·6)	27
{[Zn_2(**L**^{1})(1,4-NDC)$_2$]·MeOH}$_n$, **1**	2-fold interpenetrated 3D, sqc493 (**pcu**)	this work
{[Cu(**L**^{1})(1,4-NDC)(H_2O)]·3H_2O}$_n$, **2**	1D triple-strained helical chain	this work
{[Cd(**L**^{1})(1,4-NDC)]·2H_2O}$_n$, **3**	3-fold interpenetrated 3D, **coe** (**dia**)	this work
[{Co_2(**L**^{3})$_2$(1,4-PDA)$_2$}(H_2O)$_2$]$_n$	2D, {4^{12}·5^2·6}	14
[{Co(**L**^{3})(1,3-PDA)}(H_2O)$_2$]$_n$	2D, **sql**	14
[{Co(**L**^{3})(IPA)}(DMF)$_2$(H_2O)]$_n$	2D, **sql**	28
[{Co_2(**L**^{3})$_2$(TPA)$_2$}(DMF)$_4$]$_n$	2-fold interpenetrated 3D, **pcu**	28
{[Ni(**L**^{3})(1,4-BDC)]·2DMF}$_n$	2-fold interpenetrated 3D, **pcu**	29

 doi:10.20944/preprints202408.1890.v1

{[Co(L^3)(TDC)]·2DMF}$_n$	2-fold interpenetrated 3D	29

adman = 1- adamantanecarboxylic acid; 5-H_2NIP = 5-nitroisophthalic acid; 2,5-H_2TPD = 2,5-thiophenedicarboxylic acid; 1,3-H_2BDC = 1,3-benzenedicarboxylic acid; 5-H_2AIP = 5-aminoisophthalic acid; H_2IPA = isophthalate; H_2TPA = terephthalate; 1,2-H_2CTA = 1,2-carboxytranscinamate; 1,4-H_2PDA = 1,4-phenylene dicarboxylate; 1,3-H_2PDA = 1,3-phenylene dicarboxylate; 1,4-H_2BDC = 1,4-benzenedicarboxylic acid; H_2TDC = thiopehenedicarboxylic acid; H_2chdc = trans-1,4-cyclohexanedicarboxylic acid; H_2mip = 5-methylisophthalic acid; H_2hip = 5-hydroxyisophthalic acid.

3.9. Thermal Properties

Thermogravimetric analyses (TGA) were conducted to investigate the thermal decomposition of complexes **1** - **6**, as summarized in Table 5 and illustrated in Figure S7 - Figure S12. Complexes **1** – **6** exhibit two-step weight loss patterns corresponding to the removal of the solvents followed by the decomposition of the ligands. Notably, complex **4** displays the highest onset temperature for the removal of organic ligands, which leads to the collapse of the framework. This suggests that the self-catenated 3D framework in complex **4** may possess enhanced structural stability compared to the other complexes.

Table 5. Thermal properties of **1** - **6**.

Complex	Weight Loss of Solvent, T, °C (observed/calcd),%	Weight Loss of Ligand, T, °C (observed/calcd),%
1	MeOH, 30 - 120 (3.20/2.36)	L^1 + 1,4-NDC^{2-}, 300 - 800 (62.36/60.22)
2	3H_2O, 30 - 120 (7.11/7.90)	L^1 + 1,4-NDC^{2-}+H_2O, 240 - 900 (84.53/81.72)
3	2H_2O, 30 - 150 (4.66/5.37)	L^1 + 1,4-NDC^{2-}, 270 - 800 (80.80/81.54)
4	20-330 (15.5/15.1)	330-700 (65.2/60.7)
5	30-120 (4.3/6.7)	120-800 (70.0/79.9)
6	100-230 (4.6/3.0)	230-800 (79.5/78.6)

3.10. Luminescent Properties

The solid-state excitation and emission spectra of L^1, L^2, 1,4-H_2NDC, adipic acid, and complexes **1**, **3**, **5** and **6** were investigated at room temperature as shown in Figure S13 – Figure S17. The corresponding excitation and emission wavelengths are listed in Table 6. The free ligands L^1, L^2, 1,4-H_2NDC, and adipic acid exhibit emissions at 410, 480, 460, and 360 nm, respectively, which may be attributed to the intraligand (IL) n → π* or π → π* transitions. In contrast, complexes **1**, **3**, **5**, and **6** display emissions at 386, 381, 385, and 297 nm, respectively. Given the d^{10} electronic configuration of the Zn(II) and Cd(II) ions, which precludes significant oxidation and reduction processes, these emissions are most likely due to ligand-to-ligand charge transfer (LLCT), with possible contributions from metal-to-ligand charge transfer (MLCT) [30,31]. The observed red and blue shifts relative to the free organic compounds are likely a result of differences in ligand conformations, coordination modes, and the formation of various structural types.

Table 6. The excitation and emission wavelengths of L^1, 1,4-H_2NDC, L^2 and adipic acid and complexes **1**, **3**, **5** and **6** in solid state.

Compound	λ_{ex} (nm)	λ_{em} (nm)	Complex	λ_{ex} (nm)	λ_{em} (nm)
L^1	318	410	**1**	340	386
1,4-H_2NDC	280, 360sh	480	**3**	334	381
L^2	300	460	**5**	342	385
Adipic acid	235	360	**6**	272	297

4. Conclusions

Six new CPs have been successfully synthesized using either the angular ligand L^1 or flexible ligand L^2 in combination with dicarboxylic acids and metal salts. The results underscore the

 doi:10.20944/preprints202408.1890.v1

propensity of both angular **L**[1] and flexible **L**[2] ligands to form entangled CPs. The isomerism exhibited by ligands **L**[1] and **L**[2] significantly influences the structural entanglement observed in the resulting CPs. For instant, complexes **1** and **3** stand out as prominent examples of entangled CPs derived from the **L**[1] ligand. This study offers valuable insights into the factors that govern the formation of entangled CPs. It highlights that the judicious selection of metal ions is crucial in designing CPs based on angular **L**[1] or flexible **L**[2] ligands, especially when supported by 1,4-NDC^{2-} ligand.

Supplementary Materials: The following are available online at Preprints.org. Powder X-ray patterns (Figure S1–Figure S6). TGA curves (Figure S7–Figure S12). Excitation and emission Spectra (Figure S13–Figure S17). Crystallographic data for complexes **1** - **6** have been deposited with the Cambridge Crystallographic Data Centre, CCDC No. 2376401-2376406.

Author Contributions: Investigation, F.-J.C. and K.-M.W.; data curation, C.-Y.L; validation, S.-W.W.; review and supervision, K.B.T., M.G. and J.-D.C. All authors have read and agreed to the published version of the manuscript.

Funding: This research was funded by the National Science and Technology Council of the Republic of China: NSTC 112-2113-M-033-004.

Acknowledgments: We are grateful to the Ministry of Science and Technology of the Republic of China for support.

Conflicts of Interest: The authors declare no conflict of interest.

References

1. Batten, S.R.; Champness, N.R.; Chen, X.-M.; Garcia-Martinez, J.; Kitagawa, S.; Öhrström, L.; O'Keeffe, M.; Suh, M.P.; Reedijk, J. Terminology of metal–organic frameworks and coordination polymers. *Pure Appl. Chem.* **2013**, *85*, 1715–1724.
2. Batten, S.R.; Neville, S.M.; Turner, D.R. *Coordination Polymers: Design, Analysis and Application*; Royal Society of Chemistry: Cambridge, UK, 2009.
3. R.P. Sijbesma, R.P.; Meijer, E.W. Self-assembly of well-defined structures by hydrogen bonding. *Curr. Opin. Colloid Interface Sci.* **1999**, *4*, 24-32.
4. Li, H.-H.; Chen, Z.-R.; Li, J.-Q.; Huang, C.-C.; Zhang, Y.-F.; Jia, G.-X. Role of Spacers and Substituents in the Self-Assembly Process: Syntheses and Characterization of Three Novel Silver(I)/Iodine Polymers. *Cryst. Growth Des.* **2006**, *6*, 1813-1820.
5. Bu, X.H.; Chen, W.; Hou, W.F.; Zhang, R.H.; Brisse, F. Controlling the Framework Formation of Silver(I) Coordination Polymers with 1,4-Bis(phenylthio)butane by Varying the Solvents, Metal-to-Ligand Ratio, and Counter anions. *Inorg. Chem.* **2002**, *41*, 3477–3482.
6. Blake, A.J.; Champness, N.R.; Cooke, P.A.; Nicolson, J.E.B.; Wilson, C. Multi-modal bridging ligands; effects of ligand functionality, anion and crystallisation solvent in silver(I) co-ordination polymers. *J. Chem. Soc., Dalton Trans.* **2000**, 3811–3819.
7. Carlucci, L.; Ciani, G.; Proserpio, D.M. Polycatenation, polythreading and polyknotting in coordination network chemistry. *Coord. Chem. Rev.* **2003**, *246*, 247–289.
8. Zaman, M.B.; Smith, M.D.; zur Loye, H.-C. Two different one-dimensional structural motifs in the same coordination polymer: A novel interpenetration of infinite ladders by bundles of infinite chains. *Chem. Commun.* **2001**, *21*, 2256-2257.
9. Hsu, Y.-F.; Lin, C.-H.; Chen, J.-D.; Wang, J.-C. A Novel Interpenetrating Diamondoid Network from Self-Assembly of N,N′-Di(4-pyridyl)adipoamide and Copper Sulfate: An Unusual 12-Fold, [6 + 6] Mode. *Cryst. Growth Des.* **2008**, *8*, 1094-1096.
10. Hsu, C.-H.; Huang, W.-C.; Yang, X.-K.; Yang, C.-T.; Chhetri, P.M.; Chen, J.-D. Entanglement and Irreversible Structural Transformation in Co(II) Coordination Polymers Based on Isomeric Bis-pyridyl-bis-amide Ligands. *Cryst. Growth Des.* **2019**, *19*, 1728-1737.
11. Wu, T.-T.; Hsu, W.; Yang, X.-K.; He, H.-Y.; Chen, J.-D. Entanglement in Co(II) coordination networks: polycatenation from single net to 2-fold and 3-fold interpenetrated nets, CrystEngComm **2015**, *17*, 916-924.
12. Chhetri, P.M.; Wu, M.-H.; Hsieh, C.-T.; Yang, X.-K.; Wu, C.-M.; Yang, E.-C.; Wang, C.-C.; Chen, J.-D. A Pair of CoII Supramolecular Isomers Based on Flexible Bis-Pyridyl-Bis-Amide and Angular Dicarboxylate Ligands. *Molecules* **2020**, *25*, 201.
13. Huang, W.-C. Chen, W.-H.; Chen, C.-L. Liao, T.-T. Chen, Y.-W. Chen, J.-D. Formation of entangled Co(II) coordination polymers based on bis-pyridyl-bis-amide and angular dicarboxylate ligands: a structural comparison, *CrystEngComm* **2023**, *25*, 5575–5587.

 doi:10.20944/preprints202408.1890.v1

14. Ganguly, S.; Parveen, R.; Dastidar, P. Rheoreversible Metallogels Derived from Coordination Polymers. *Chem. Asian J.* **2018**, *13*, 1474-1484.
15. Kumar, G.; Turnbull, M.M.; Thakur, V.; Gupta, S.; Trivedi, M.; Kumar, R.; Husain, A, Solvothermal synthesis, structural characterization, DFT and magnetic studies of a dinuclear paddlewheel Cu(II)-metallamacrocycle. *J. Molecular Struct.* **2020**, *1201*, 127193.
16. Bruker AXS. APEX2, V2008.6; SAD ABS V2008/1; SAINT+ V7.60A.; SHELXTL V6.14; Bruker AXS Inc.: Madison, WI, USA, 2008.
17. Sheldrick, G.M. Crystal structure refinement with SHELXL. *Acta Cryst.* **2015**, *71*, 3–8.
18. Addison, A.W.; Rao, T.N.; Reedijk, J.; van Rijn, J.; Verschoor, G.C. Synthesis, structure, and spectroscopic properties of copper(II) compounds containing nitrogen–sulphur donor ligands; the crystal and molecular structure of aqua[1,7-bis(N-methylbenzimidazol-2′-yl)-2,6-dithiaheptane]copper(II) perchlorate. J. Chem. Soc., Dalton Trans. **1984**, 1349-1356.
19. Blatov, V.A.; Shevchenko, A.P.; Proserpio, D.M. Applied topological analysis of crystal structures with the program package ToposPro. *Cryst. Growth Des.* **2014**, *14*, 3576–3586.
20. Yang, X.-K.; Chang, M.-N.; Hsing, J.-F.; Wu, M.-L.; Yang, C.-T.; Hsu, C.-H.; Chen, J.-D. Synthesis, crystal structures and thermal properties of six Co(II) and Ni(II) coordination polymers with mixed ligands: Formation of a quadruple-strained helical nanotube. *J. Molecular Struct.* **2018**, *1171*, 340-348.
21. Cheng, P.-C; Kuo, P.-T.; Xie, M.-Y.; Hsu, W.; Chen, J.-D. Structure-directing roles of auxiliary polycarboxylate ligands in the formation of Zn(II) and Cd(II) coordination polymers based on a flexible N,N′-di(3-pyridyl)dodecanedioamide. *CrystEngComm* **2013**, *15*, 6264–6272.
22. Li, D.-S.; Zhao, J.; Wu, Y.-P.; Liu, B.; Bai, L.; Zou, K.; Du, M. Co5/Co8−Cluster-Based Coordination Polymers Showing High-Connected Self-Penetrating Networks: Syntheses, Crystal Structures, and Magnetic Properties. *Inorg. Chem.* **2013**, *52*, 8091−8098.
23. Yang, X.-K.; Chen, J.-D. Crystal-to-crystal transformation and linker exchange in Cd(II) coordination polymers based on flexible bis-pyridyl-bis-amide and 1,4-naphthalenedicarboxylate. *CrystEngComm* **2019**, *21*, 7437–7446.
24. Lakshmanan, V.; Lai, Y.-T.; Yang, X.-K. Govindaraj, M.; Lin, C.-H.; Chen, J.-D. Eight-Fold Interpenetrating Diamondoid Coordination Polymers for Sensing Volatile Organic Compounds and Metal Ions. *Polymers* **2021**, *13*, 3018.
25. Wang, X.-L.; Wu, X.-M,; Liu, G.-C.; Lin, H.-Y.; Wang, X. A series of pyridyl-amide-based ZnII/CdII coordination polymers and their polypyrrolefunctionalized composite materials for tuning their photocatalytic properties. *RSC Adv.* **2016**, *6*, 85030.
26. Liu, G.-C.; Li, Y.; Xiong, Y.; Liu, X.-X.; Li, Q.-M.; Zhang, J.-W.; Lin, H.-Y.; Li, X.-W. Spacers-directed structural diversity of Co(II)/Zn(II) complexes based on S-/O-bridged dipyridylamides: electrochemical, fluorescent recognition behavior and photocatalytic properties. *J. Coord. Chem.* **2018**, *71*, 483-501.
27. Wang, X.-L.; Wu, X.-M.; Liu, G.-C.; Chen, N.-L.; Lin, H.-Y.; Wang, X. Structural Diversity and Properties of Six ZnII/CdII Coordination Polymers Based on an O-Bridged Semi-Rigid Bis-pyridyl-bis-amide and Different Dicarboxylates. *Aust. J. Chem.* **2016**, *69*, 846-855.
28. Ganguly, S.; Mukherjee, S.; Dastidar, P. Single-Crystal-to-Single-Crystal Breathing and Guest Exchange in Co(II) Metal−Organic Frameworks. *Cryst. Growth Des.* **2016**, *16*, 5247−5259.
29. Rao, P.C.; Chaudhary, S.P.; Arjun, U.; Kuznetsov, D.; Nath, R.C.; Mandal, S. Magnetic diversity in three-dimensional two-fold interpenetrated structures: a story of two compounds. *Dalton Trans.* **2017**, *46*, 12804.
30. Sun, D.; Yan, Z.-H.; Blatov, V.A.; Wang, L.; Sun, D.-F. Syntheses, Topological Structures, and Photoluminescences of Six New Zn(II) Coordination Polymers Based on Mixed Tripodal Imidazole Ligand and Varied Polycarboxylates. *Cryst. Growth Des.* **2013**, *13*, 1277–1289.
31. Yang, J.-X.; Xin, Z.; Y.-Y. Qin; Yao, Y.-G. N-Donor Auxiliary Ligand Influence on the Coordination Mode Variations of V- Shaped Triazole Dicarboxylic Acid Ligand Affording Seven New Luminescent Zn(II) Compounds with Variable Structural Motifs. *Cryst. Growth Des.* **2020**, *20*, 6366–6381.